Supporting Information

Lewis et al. 10.1073/pnas.1317002110

SI Methods

Cell Culture. Sf9 cells were used for baculovirus generation and protein expression. The cells were grown at 28 °C in a suspension culture using Sf-900 II SFM (Invitrogen), supplemented with 0.1% pluronic acid (Sigma). A stable *Drosophila* cell line (648-1B6) expressing luciferase under the control of the drosomycin promoter was established from S2 cells (Invitrogen) and was a kind gift from Jean-Luc Imler (Institut de Biologie Moléculaire et Cellulaire, Strasbourg, France) (1). These cells were grown at 28 °C in Express Five SFM (Invitrogen), supplemented with 2 mM L-glutamine, 1% penicillin/streptomycin, and 0.5 μM puromycin. HEK293ET (human embryonic kidney 293 EBNA-T) cells were grown at 37 °C (5% CO_2, 100% humidity) in DMEM (Invitrogen), supplemented with 10% (vol/vol) FCS (Invitrogen) and 2 mM L-glutamine.

Luciferase Assay. S2 cells were placed into 96-well plates and stimulated overnight by the addition of purified recombinant Spätzle (Spz) (or mutant Spz) to the culture medium. Cells were lysed using Passive Lysis buffer (Promega), and the activity was measured using a GloMax luminometer (Promega) immediately after the addition of the D-Luciferin substrate (Biosynth). All assays were performed three times in triplicate. Data are shown as mean ± SD of the mean.

Sedimentation Velocity Analytical Ultracentrifugation. All analytical ultracentrifugation experiments were performed on an Optima XL-A/I (Beckman Coulter) centrifuge equipped with a four-hole titanium rotor, double-sector centerpieces, and an interference optical system for data acquisition. Sedimentation velocity runs were performed at 45,000 rpm with 3-min intervals between scans for a total of 190 scans at 20 °C. The sample volume was 400 μL. Data were analyzed using Sedfit software (2). The partial specific volumes, buffer density, and viscosity were estimated using SEDNTERP software (3).

Isothermal Titration Calorimetry. Measurements were carried out using a Microcal ITC 200 microcalorimeter at 25 °C by injecting C106 at a concentration of 524 μM into the measuring cell containing $Toll_{N13}$–VLR construct at a concentration of 46.2 μM. In the reverse setup, $Toll_{N13}$–VLR at a concentration of 392 μM was injected into C106 at a concentration of 17 μM. Twenty 2-μL injections were made at 3-min intervals into a cell containing 300 μL at a stirring speed of 300 rpm. Data were subsequently imported into ORIGIN software and processed as recommended by the manufacturer. Protein concentrations were determined by amino acid analysis for maximum accuracy.

Mass Spectrometry. Protein samples were buffer exchanged into 200 mM ammonium acetate, pH 6.9, using micro bio-spin chromatography columns (Bio-Rad). A nano-electrospray ionization source was used to infuse samples into the LCT Premier mass spectrometer (Micromass U.K. Ltd./Waters Corp.) via in-house fabricated gold-palladium–coated borosilicate capillaries using a voltage of 1.8 kV at 10 μM protein concentration. The following instrument parameters were used: cone voltage 30 V, source temperature 80 °C. Data were processed by the use of MassLynx v.4.1 software supplied with the mass spectrometer. The instrument was calibrated using a separate introduction of aqueous CsI at 1 mg/mL.

Data Collection, Phase Determination, and Model Refinement. The best dataset was collected at a resolution of 2.3 Å at beamline I24 of the Diamond light source Synchrotron Facility (DLS, Didcot, UK). Oscillation images were recorded at 0.15° over 360 degrees using a Pilatus detector and a beam width of 50 μm. These were integrated, and reflection intensities were merged using the XDS package (4) and scaled using Aimless (5). Only 1,800 (270°) were used during scaling to minimize the effect of radiation damage.

The data were severely anisotropic and required ellipsoidal truncation and anisotropic scaling using the diffraction anisotropy server (6) on the XDS processed data. The spread in values of the three principle components was 28.07 $Å^2$. In decreasing order, the three components were 17.42, −7.77, and −10.65 $Å^2$. The resolution limits at which F/sigma dropped below an arbitrary cutoff of 3.0 were 2.3 Å along a* and c* and, 3.2 Å along b*. Out of 162,698 reflections 35,925 were discarded because they fell outside the specified ellipsoid with dimensions 1/2.3, 1/3.2, 1/2.3 $Å^{-1}$ along a*, b*, and c*, respectively. These discarded reflections had an average F/sigma of 0.18. Then, 126,773 reflections remained after ellipsoidal truncation. Anisotropic scale factors were then applied to remove anisotropy from the dataset. Lastly, an isotropic B of −25.19 $Å^2$ was applied to restore the magnitude of the high-resolution reflections diminished by anisotropic scaling.

Molecular replacement (MR) was undertaken using Phaser (7), with models that were improved using Phenix Morph (8). The initial ligand model was taken from the crystal structure of refolded Spz (9) whereas the receptor models were based on the crystal structure of $Toll_{N6}$–VLR (10, 11), a homology model for Toll residues 229–399 based on the crystal structure of the Nogo receptor (12, 13), and the VLR leucine-rich repeat C-terminal domain (LRRCT) cap originally used by Kim et al. (14). Structure solutions by MR with Spz C106 had C-alpha clashes in the wings and were rejected in the packing test unless the wings were deleted.

Refinement was carried out using Refmac (15), Phenix Refine (8), and Buster (16). Despite the anisotropically scaled data, no extra density was found for the missing 12% amino acids of the complex. Expanding data to P1 and doubling the ASU did not yield better electron density.The R-factors reached suggest that these atoms are not ordered in the crystal. The quality of the structure was assessed with Molprobity (17).

1. LeMosy EK, Tan YQ, Hashimoto C (2001) Activation of a protease cascade involved in patterning the Drosophila embryo. *Proc Natl Acad Sci USA* 98(9):5055–5060.
2. Schuck P (2000) Size-distribution analysis of macromolecules by sedimentation velocity ultracentrifugation and lamm equation modeling. *Biophys J* 78(3):1606–1619.
3. Laue TM, Shah BD, Ridgeway TM, Pelletier SL (1992) Computer-aided interpretation of analytical sedimentation data for proteins. *Analytical Ultracentrifugation in Biochemistry and Polymer Science*, eds Harding SE, Rowe AJ, Horton JC (Royal Society of Chemistry, Cambridge, UK), pp 90–125.
4. Kabsch W (2010) Xds. *Acta Crystallogr D Biol Crystallogr* 66:125–132.
5. Anonymous; Collaborative Computational Project, Number 4 (1994) The CCP4 suite: Programs for protein crystallography. *Acta Crystallogr D Biol Crystallogr* 50(Pt 5): 760–763.
6. Strong M, et al. (2006) Toward the structural genomics of complexes: Crystal structure of a PE/PPE protein complex from Mycobacterium tuberculosis. *Proc Natl Acad Sci USA* 103(21):8060–8065.
7. McCoy AJ, et al. (2007) Phaser crystallographic software. *J Appl Cryst* 40(Pt 4):658–674.
8. Adams PD, et al. (2010) PHENIX: A comprehensive Python-based system for macromolecular structure solution. *Acta Crystallogr D Biol Crystallogr* 66(Pt 2):213–221.

9. Hoffmann A, et al. (2008) Biophysical characterization of refolded Drosophila Spätzle, a cystine knot protein, reveals distinct properties of three isoforms. *J Biol Chem* 283(47):32598–32609.
10. Gangloff M, Moreno A, Gay NJ (2013) Liesegang-like patterns of Toll crystals grown in gel. *J Appl Cryst* 46(Pt 2):337–345.
11. Gangloff M, Arnot CJ, Lewis M, Gay NJ (2013) Functional insights from the crystal structure of the N-terminal domain of the prototypical toll receptor. *Structure* 21(1): 143–153.
12. He XL, et al. (2003) Structure of the Nogo receptor ectodomain: A recognition module implicated in myelin inhibition. *Neuron* 38(2):177–185.
13. Barton WA, et al. (2003) Structure and axon outgrowth inhibitor binding of the Nogo-66 receptor and related proteins. *EMBO J* 22(13):3291–3302.
14. Kim HM, et al. (2007) Crystal structure of the TLR4-MD-2 complex with bound endotoxin antagonist Eritoran. *Cell* 130(5):906–917.
15. Murshudov GN, Vagin AA, Dodson EJ (1997) Refinement of macromolecular structures by the maximum-likelihood method. *Acta Crystallogr D Biol Crystallogr* 53(Pt 3):240–255.
16. Smart OS, et al. (2012) Exploiting structure similarity in refinement: automated NCS and target-structure restraints in BUSTER. *Acta Crystallogr D Biol Crystallogr* 68(Pt 4): 368–380.
17. Chen VB, et al. (2010) MolProbity: All-atom structure validation for macromolecular crystallography. *Acta Crystallogr D Biol Crystallogr* 66(Pt 1):12–21.

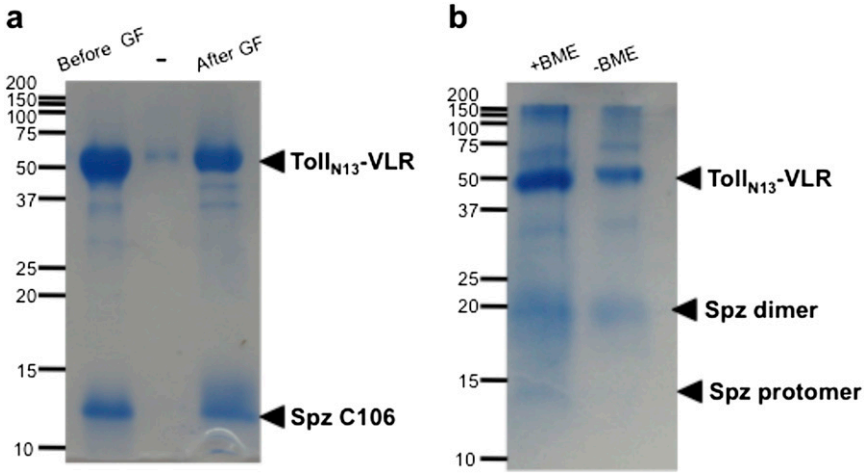

Fig. S1. Purity and integrity of the Toll$_{N13}$–VLR–Spz complex. (*A*) A reducing 15% Coomassie-stained SDS/PAGE gel showing protein samples submitted to AUC [before and after gel-filtration (GF)] before crystallization reveals an intact although blurry band for Spz (12 kDa), a broad band for Toll$_{N13}$–VLR (about 55 kDa), and some minor contaminants (around 30–50 kDa). (*B*) Dissolved crystals were also analyzed on a 15% Coomassie-stained SDS/PAGE gel in reducing (+BME) and nonreducing conditions (–BME). BME stands for β-mercaptoethanol.

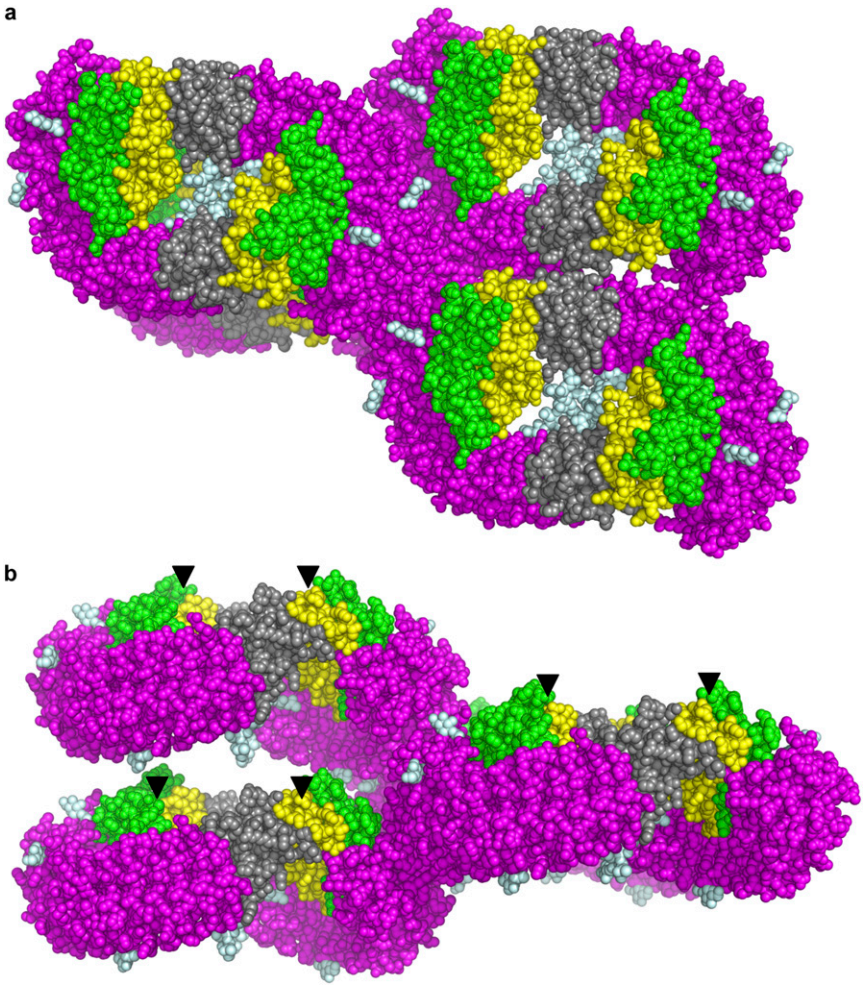

Fig. S2. Crystal packing leaves channels able to accommodate the invisible lobes of Spz. (*A*) Top view along the twofold axis and (*B*) a 90° rotated side view of the crystal packing with surface representations of $Toll_{N13}$–VLR shown in magenta and gray and Spz dimer in yellow and green, respectively. Glycan structures are depicted in pale cyan spheres. Although the packing is dense (solvent content 50% assuming 724 residues), the side view orientation possesses suitable gaps to fit the missing Spz loops (indicated as black triangles).

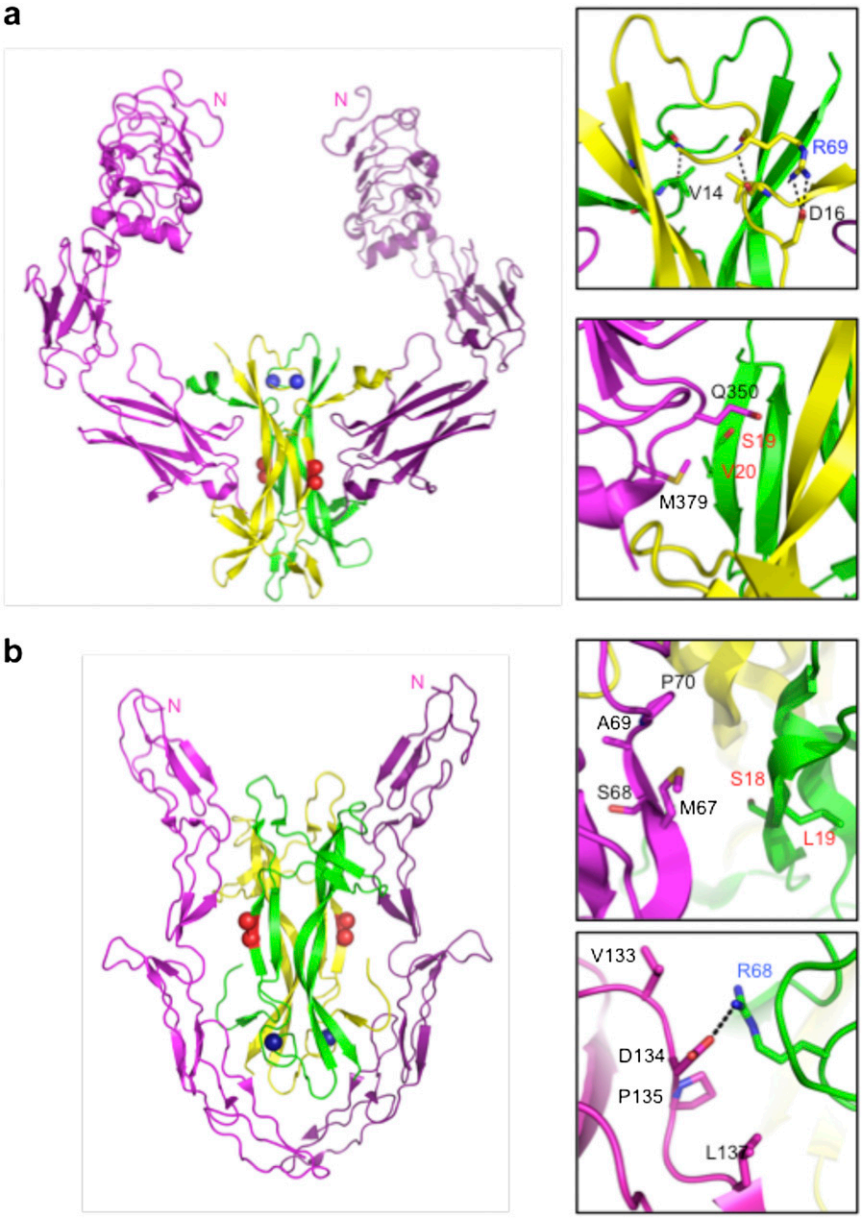

Fig. S3. Binding mode of mammalian neurotrophins. Schematic representation of receptors in magenta and growth factors in green and yellow. Red spheres represent residues equivalent to Spz R14/K15:S19/V20 in NGF; and, S18/ L19 in NT3. Blue spheres show the location of the residues that align with Spz D55:R69 in NGF; and R68 in NT3. (*A*) hNGFb dimer bound to tyrosine receptor kinase hTrkA in a 1:2 stoichiometry (1). R69 stabilizes the NGF dimer without any involvement in TrkA receptor binding. S19/V20 in each protomer interact with receptor in a symmetric complex. (*B*) hNT3 dimer bound to neurotrophin receptor $p75^{NTR}$ in a 1:2 stoichiometry (2). Note that the orientation of bound NT3 is head up compared with NGF depicted above. This binding mode involves both areas S18/L19 as part of a hydrophobic patch and R68 in a salt bridge with D134.

1. Wehrman T, et al. (2007) Structural and mechanistic insights into nerve growth factor interactions with the TrkA and p75 receptors. *Neuron* 53(1):25–38.
2. Gong Y, Cao P, Yu HJ, Jiang T (2008) Crystal structure of the neurotrophin-3 and p75NTR symmetrical complex. *Nature* 454(7205):789–793.

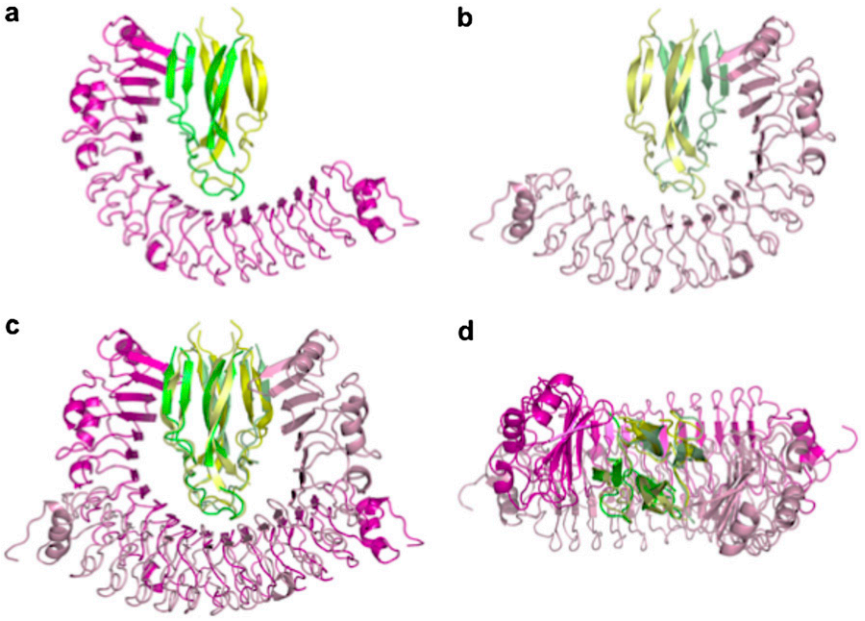

Fig. S4. The crystal structure of Spz-bound $Toll_{N13}$–VLR is not compatible with a symmetrical 2:1 complex similar to mammalian neurotrophin receptor complexes. Spz chain L of complex (*A*) is aligned with Spz chain M of complex (*B*) to form *C* and *D*, which are side and top views, respectively, of the clashing Toll dimer in an impossible 2:1 complex. The superposition and graphics were generated using Pymol (1).

1. DeLano WL (2002) *The PyMOL Molecular Graphics System* (DeLano Scientific, San Carlos, CA).

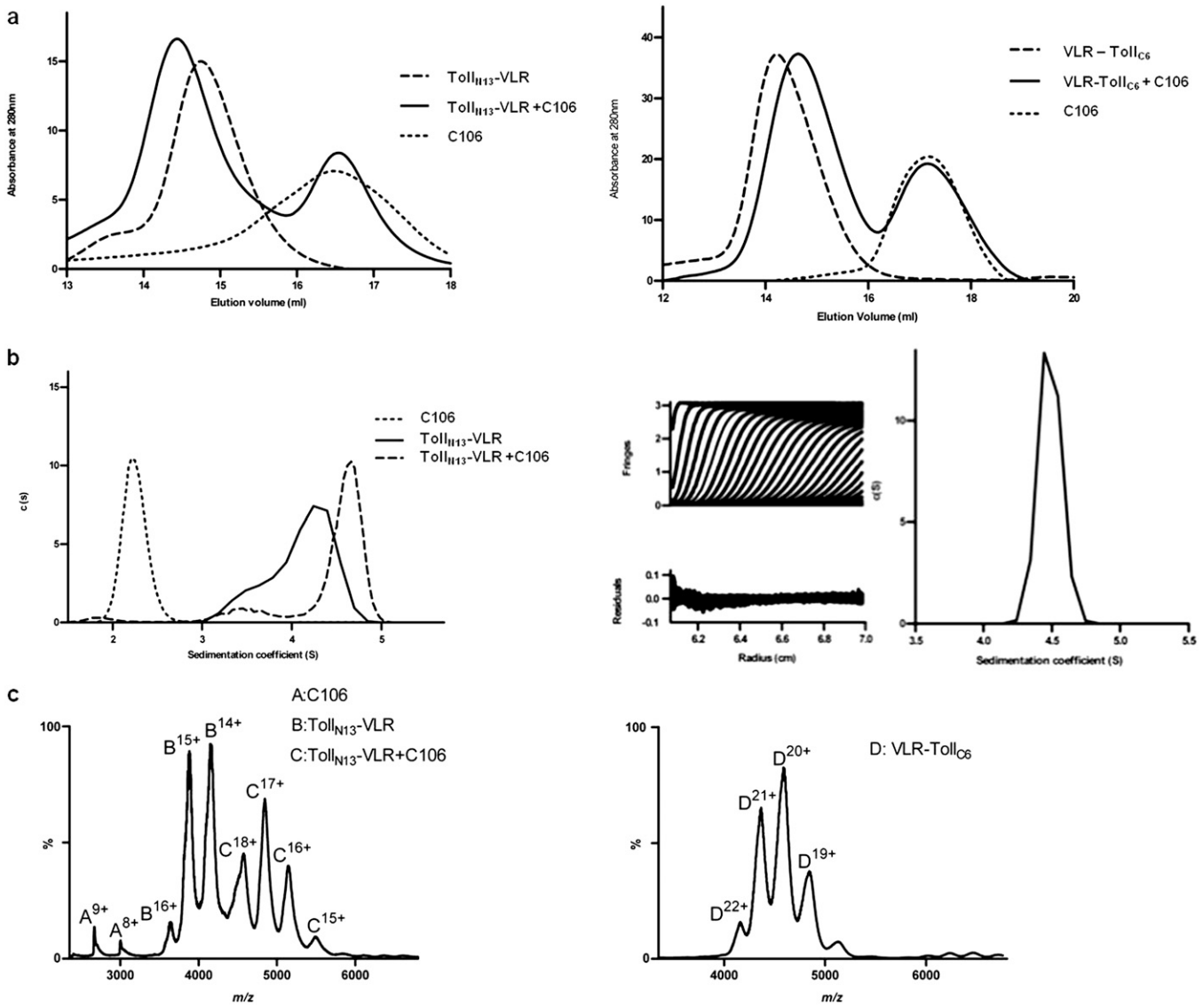

Fig. S5. Biophysical analysis of Toll$_{N13}$–VLR and VLR–Toll$_{C6}$. Spz C106 binds Toll$_{N13}$–VLR in contrast to VLR–Toll$_{C6}$ whereas both remain monomeric in solution. Toll$_{N13}$–VLR is shown on the *Left* and VLR–Toll$_{C6}$ on the *Right*. (*A*) Gel-filtration profiles. Toll$_{N13}$–VLR does left-shift, indicating the formation of a stable 1:1 complex whereas there is a slight right-shift of VLR–Toll$_{C6}$ in the presence of C106, which might reflect a transient interaction as for Toll$_{N6}$–VLR. (*B*) Analytical ultracentrifugation profiles. Toll$_{N13}$–VLR at 4.2 S (with a contaminant at 3.5 S) shifts toward a higher molecular weight species in complex with C106 (at about 4.6 S). VLR–Toll$_{C6}$, which does not bind C106, is shown with its fit and residuals after fitting to a c(S) model in SEDFIT and the distribution of sedimentation coefficients. VLR–Toll$_{C6}$ at 2.7 μM sedimented at 4.5 S. (*C*) Mass spectrometry analysis detects the Toll$_{N13}$–VLR–C106 monomer at about 58 kDa, C106 at 24 kDa, and their complex at 82 kDa whereas VLR–Toll$_{C6}$ is a monomer of about 92 kDa.

Table S1. Interfaces in the Toll$_{N13}$–VLR–Spz C106 crystal structure

Chains	Interface area, Å^2	Δ^iG, kcal/mol	Δ^iG *P* value	Complexation significance score
R-(L/M)	1589.2	1.4	0.629	n.d.
L-M	1367.0	−12.2	0.270	1.000
R-M	1144.1	4.8	0.875	1.000
R-L	532.9	−3.0	0.272	1.000
L-R*	550.1	−3.4	0.234	n.d.

The analysis generated by PDBePISA (1) presented below does not include glycan interactions. n.d., not determined.

1. Krissinel E, Henrick K (2007) Inference of macromolecular assemblies from crystalline state. *J Mol Biol* 372(3):774–797.

Table S2. Hydrogen bonds in Toll-Spz complex

	$Toll_{N13}$–VLR chain R	Distance, Å	Spz chains M and L
1	R:ARG 105[NH1]	2.76	M:GLY 0[O]
2	R:GLN 103[NE2]	3.53	M:VAL 1[O]
3	R:ARG 101[NH2]	2.54	M:GLY 2[O]
4	R:ARG 101[NE]	3.05	M:SER 4[OG]
5	R:ARG 105[NH2]	2.83	M:SER 12[O]
6	R:ARG 66[NH1]	3.64	M:ARG 14[O]
7	R:GLN 44[NE2]	3.66	M:TYR 18[OH]
8	R:ARG 106[NE]	3.3	M:GLU 48[OE2]
9	R:ARG 182[NH1]	2.77	M:ASP 55[OD1]
10	R:ARG 304[NH2]	3.36	M:ALA 58[O]
11	R:ASN 302[ND2]	3.31	M:ASN 59[O]
12	R:ASN 302[ND2]	2.96	M:ASN 59[OD1]
13	R:ARG 304[NH1]	3.08	M:PHE 60[O]
14	R:ARG 304[NH2]	2.88	M:PHE 60[O]
15	R:GLU 180[OE2]	2.73	M:ARG 7[NH1]
16	R:GLU 61[OE2]	3.19	M:LYS 15[NZ]
17	R:MET 301[SD]	3.88	M:ASN 59[ND2]
18	R:ARG 304[O]	3.16	M:GLN 62[NE2]
19	R:ARG 299[NH1]	2.79	L:PHE 60[O]
20	R:ASN 227[ND2]	2.98	L:GLN 62[O]
21	R:ILE 250[N]	3.12	L:GLN 62[OE1]
22	R:GLN 225[NE2]	2.85	L:GLN 62[OE1]
23	R:ASP 251[N]	3.76	L:GLN 62[OE1]
24	R:MET 49[N]	2.75	L:GLN 74[OE1]
25	R:ASP 251[OD2]	2.74	L:GLN 62[N]
26	R:ILE 250[O]	3	L:GLN 62[NE2]
27	R:GLU 203[OE1]	2.79	L:TYR 64[OH]
28	R:PRO 47[O]	3.18	L:GLN 74[NE2]

Table S3. Salt bridges in Toll-Spätzle complex

	$Toll_{N13}$–VLR chain R	Distance, Å	Spz chain M
1	R:ARG 105[NH2]	3.44	M:GLU 48[OE1]
2	R:ARG 105[NE]	3.97	M:GLU 48[OE2]
3	R:ARG 105[NH2]	3.7	M:GLU 48[OE2]
4	R:ARG 106[NE]	3.3	M:GLU 48[OE2]
5	R:ARG 106[NH2]	3.8	M:GLU 48[OE2]
6	R:ARG 182[NH1]	2.77	M:ASP 55[OD1]
7	R:ARG 182[NH2]	3.7	M:ASP 55[OD2]
8	R:ARG 182[NH1]	3.15	M:ASP 55[OD2]
9	R:GLU 180[OE1]	2.98	M:ARG 7[NH1]
10	R:GLU 180[OE2]	2.73	M:ARG 7[NH1]
11	R:GLU 180[OE2]	3.74	M:ARG 7[NH2]
12	R:GLU 53[OE2]	3.15	M:ARG 14[NE]
13	R:GLU 53[OE1]	3.92	M:ARG 14[NE]
14	R:GLU 51[OE1]	3.36	M:ARG 14[NH1]
15	R:GLU 51[OE1]	3.17	M:ARG 14[NH2]
16	R:GLU 61[OE2]	3.19	M:LYS 15[NZ]

Table S4. Isothermal titration calorimetry on $Toll_{N13}$–VLR–Spz C106

Syringe		Cell		Experimental values				
Protein	Concentration, μM	Protein	Concentration, μM	*N*	K_D	ΔH, kcal/mol	ΔS, cal/mol/K	ΔG, kcal/mol
C106	524	$Toll_{N13}$VLR	46	0.96	33.6 ± 0.3	−13.2	−10.3	−10.2
C106	297	$Toll_{N13}$VLR	36	1.01	56.8 ± 0.2	−13.9	−13.7	−9.9
$Toll_{N13}$VLR	392	C106	17	1.09	50.5 ± 0.1	−7.0	9.97	−4.0

Purified Spz C106 was titrated into the ITC measuring cell containing $Toll_{N13}$–VLR protein resulting in the formation of a complex of one truncated ectodomain binding a single Spz dimer with a dissociation constant between 30 and 50 nM (depending on the protein preparation) comparable with the affinity of full-length ectodomain (1). In the reciprocal titration in which $Toll_{N13}$–VLR was injected into Spz C106, a complex with the same stochiometry and dissociation constant was observed. A summary table of the thermodynamic parameters is shown.

1. Weber AN, Moncrieffe MC, Gangloff M, Imler JL, Gay NJ (2005) Ligand-receptor and receptor-receptor interactions act in concert to activate signaling in the Drosophila toll pathway. *J Biol Chem* 280(24):22793–22799.

Table S5. Cloning and mutagenesis primers

	Sequence (5′–3′)	Orientation	T_m, °C
Cloning			
Toll(BamHI-Met1)	act acg gat cca tga gtc gac taa agg gct cc	Forward	78
Toll(Leu228-NheI)	Tag cta gct agc aaa ttg agc tgc ttc agc tt	Reverse	74
Toll(Leu397-NheI)	Tag cta gct agc cag acg cag atc cgt cag	Reverse	76
Toll(Ile723–NheI)	TGC TAG CTA GCT ATA TCC AAA TGG GTG AGA TT	Reverse	69
Toll (NheI-Asp231)	TAG CTA GCT AGC AAT CAA CTG CAC AAC CTC ACC	Forward	74
Toll (Aln801-AgeI)	ACT ACC GGT CGC CGG ACA AAT GTC GTT GGT	Reverse	80
VLR(NheI-Asn133)	Ata gct agc aac cag ctg aag tct gtt cct gat ggg att ttt gat cgc ctg acc agc ttg cag aaa att tgg ctt cat aca	Forward	91
VLR(Thr200-AgeI)			
Fc (AgeI-TEV-E45)*	act acc ggt gaa aac ctg tat ttt cag ggc gag cccc aaa tct tgt gac aaa	Forward	85
Fc(K276-XbaI-His×6-STOP- NotI)	atc cag cgg ccg cct agt gat ggt gat ggt gat ggt g	Reverse	88
Mutagenesis			
Spz R14A/K15A	CCT TTG CAG GAG CAT CGC GGC GCT GGT GTA CCC AAA AAA GGG C	Forward	88
Spz D55R	GAA GGA GCG GAT CAA CCC TGT CGC TTC GCC GCC AAC TTT C	Forward	82

Table S6. X-ray diffraction data collection and refinement statistics

Data collection	
Space group	C2
Cell parameters	
a, b, c, Å	198.2, 57.2, 70.5
α, β, γ, °	90.0, 97.8, 90.0
Resolution, Å	43.97–2.35 (2.43–2.35)*
No. of observations	164,263 (126,773)†
No. of unique reflections	32,800 (32,505)†
R_{merge}, %‡	0.102
R_{merge}, %†	0.082 (0.783)†
$I/\sigma(I)$	7.5
I/σ(I)†	11.5 (2.6)†
Completeness, %	99.7 (99.9)*
Completeness, %†	74.8 (32.9)†
Mean multiplicity	5.0 (5.2)*
Mean multiplicity†	3.9 (1.9)†
Refinement	
Resolution, Å	49.12–2.35
No. of reflections (total)	24,588
No. of reflections (test)	1,256
R_{work}, %§	19.5
R_{free}, %¶	22.7
No. of atoms	4,934
Protein	4,576
Heterogen atoms	254
Solvent atoms	104
Mean B, Å^2	59.7
rmsd	
Bond lengths, Å	0.01
Bond angles, °	1.11
Molprobity	
Clashscore, all atoms	3.1 (100th percentile)
Ramachandran favored, %	93.7
Ramachandran outliers, %	0.5
Cruickshank DPI	
Based on R_{work}, Å	0.482
Cruickshank DPI	
Based on R_{free}, Å	0.260

*Numbers in parentheses refer to the highest resolution shell.

†Statistics after elliptical truncation prompted by severe anisotropy.

‡$R_{merge} = \sum hkl(\sum i(|I\ hkl,I - \langle I\ hkl\rangle|))/\sum hkl,i\ \langle I\ hkl\rangle$, with I *hkl,i* the intensity of an individual measurement of the reflection with Miller indices *h*, *k* and *l*, and $\langle I\ hkl\rangle$ the mean intensity of that reflection. Value calculated for $I > -3\sigma(I)$.

§$R_{work} = \sum hkl(||Fobshkl| - |Fcalchkl||)/|Fobshkl|$, where |Fobs*hkl*| and |Fcalc*hkl*| are the observed and calculated structure factor amplitudes.

¶R_{free} is calculated as R_{work} with 5% reflections omitted from the refinement process.